

Structural, electronic, elastic properties and phase transitions of Mg₂Si from first-principles calculations

HAI RONG WANG^{a,b}, DECONG LI^b, HONGCHAN CHEN^a, YONG YANG^b, SHUKANG DENG^{a*}, ZUMING LIU^a

^aEducation Ministry Key Laboratory of Renewable Energy Advanced Materials and Manufacturing Technology, Yunnan Normal University, Kunming, Yunnan Province, 650092, P.R. China

^bCollege of Optoelectronic Engineering, Yunnan Open University, Kunming, Yunnan Province, 650223, China

Structural and electronic properties of Mg₂Si under high pressures are investigated based on density functional theory. The calculations found that Mg₂Si undergoes two pressure-induced phase transitions: anti-fluorite→anti-cotunnite→Ni₂In-type. The dependence of the elastic properties on pressure in three structures is further analyzed. The band structures show that for the anti-fluorite structure that the pressure leads to the change in the energy dispersion of lowest conduction band but the energy dispersion relations of the valence band top hardly be changed. This indicates that the conduction bands for the anti-fluorite structure are influenced by the pressure whereas the valence bands are not much affected.

(Received April 8, 2018; accepted February 12, 2019)

Keywords: Mg₂Si, Transition phase, Elastic properties, Electronic structure, First-principle calculations

1. Introduction

Due to its light weight, high melting temperature, high hardness, low density and low thermal expansion coefficient [1], magnesium alloys have attracted much attention by their (potential) use in the domains of aerospace, automobile and electronic industry. On the other hand, Mg₂Si and its related compounds, with high Seebeck coefficient, high electrical conductivity and low lattice thermal conductivity, are good candidates for high performance thermoelectric materials [2-5]. Recently, Liu *et al.* [6] showed that the Sb-doped n-type Mg₂Sn_xSi_{1-x} compounds had proven to possess the high ZT of 1.3 at 700 K.

A lot of research has been directed at the wide variety of physical properties of anti-fluorite Mg₂Si such as the structural and electronic properties [7], the thermoelectric properties [2], experimental and theoretical research of doped Mg₂Si [8-11]. At ambient conditions, Mg₂Si crystallizes and is composed of one molecular unit per primitive cell and four formulas per conventional cell (space group Fm-3m) in the cubic anti-fluorite structure. In 1964, Cannon and Conlin [12] experimentally found that Mg₂Si undergoes a phase transition to a hexagonal lattice at a pressure above 2.5 GPa and a temperature above 900 °C. Recently, Hao *et al.* [13] presented the experimental results of high-pressure structural phase transformations on Mg₂Si, and found that Mg₂Si transforms from the cubic anti-fluorite (Fm3m) structure to anti-cotunnite (Pnma) structure at 7.5 GPa and then to Ni₂In-type (P63/mmc) structure at about 21.3 GPa. In the theoretical works, researchers have studied [15] the phase transitions, electronic structures and optical properties of Mg₂Si under high pressure using the first-principles

density functional theory. But they did not present the detailed information for the effect of pressure on the electronic structure of Mg₂Si. Moreover, until now, little experimental and theoretical research has been done on elastic properties and thermodynamic properties of Mg₂Si under high pressure.

It is well known that pressure is an important parameter to tune physical properties. High-pressure research can improve our fundamental understanding of atomic and molecular interactions in solids. The studies indicated that the application of pressure can influence thermoelectric property of materials. Meng *et al.* [16, 17] reported for Sr₈Ga₁₆Ge₃₀ clathrate an improvement by at least a factor of 3 in the dimensionless thermoelectric figure of merit at pressure up to 7GPa at room temperature. On the other hand, pressure can improve the mechanical properties of materials. Martin *et al.* [18] suggest that once improved behavior is found by means of pressure tuning, attempts can be made to reproduce this behavior by means of chemical tuning, or by other means. Therefore, it is meaningful for us to investigate the physical properties of Mg₂Si at high pressure.

In this work, we report the results of the first principles calculations of Mg₂Si with different structures under high pressures. The structures are optimized by full relaxation and the lattice parameters are obtained. The crystal structural transformations of Mg₂Si are investigated under hydrostatic pressure. The most stable structure is determined at a finite pressure and volume based on the computed Gibbs free energy. The elastic constants are calculated, the bulk moduli, shear moduli, Young's moduli and Poisson ratio value are derived; Debye temperature is calculated and discussed. The researches of this paper have some theoretical guidance effect on development and

application for Mg₂Si.

2. Computational approach

In this study, the first-principles calculations were performed using the plane-wave pseudo-potential density functional theory method and implemented in the Serial Total Energy Package (CASTEP) [19]. The configurations of valence electrons are selected as Mg 2p⁶3s² and Si 3s²3p² when describing the ion solid interaction with the valence electrons and the other orbital electrons are calculated as core electrons. We used the generalized gradient approximation (GGA) with the Perdew-Burke-Ernzerhof (PBE) [20] to the exchange–correlation potential and the cutoff energy for plane wave expansion of the wave functions was set at 400 eV. The self-consistent calculations are carried out with 9×9×9, 7×9×6, 15×15×10 Monkhorst-pack [21] sampling of space for the Fm-3m, Pnma and P6₃/mmc phases. The self-consistent convergence of the total energy is at 10⁻⁶ eV/Atom and the maximum force on the atom is below 10⁻⁴ eV/Å. To optimize the geometry, we minimize the energy with respect to volume and atomic coordinates. Electronic, structural, and elastic properties were calculated at the minimum energy configurations.

3. Results and discussions

3.1. Structural properties and structure stabilities

We examine the ground state structural stability at 0 K and 0 GPa conditions. Total energy versus volume data for the anti-fluorite, anti-cotunnite and Ni₂In-type structures Mg₂Si are shown in Fig. 1. It is revealed that the anti-fluorite has the lowest total energy among three

Mg₂Si structures, indicating that the anti-fluorite structure is the stable ground state phase while the anti-cotunnite and Ni₂In-type structures of Mg₂Si are considered to be metastable.

The ground-state crystal structure of Mg₂Si is successfully obtained by optimizing the lattice constant and the obtained values are then used as the starting point to investigate the structural properties. The calculated lattice parameters for three structure types of Mg₂Si are listed in Table 1, which also includes the available experimental and theoretical data for comparison [11, 13, 15, 22]. Our results are excellent agreement with the previous theoretical results at 0 GPa. The comparison with experimental data shows an overestimation of the lattice constants. It is well known that the exchange-correlation energy functional for GGA can overestimate the bond strength and result in larger lattice parameters.

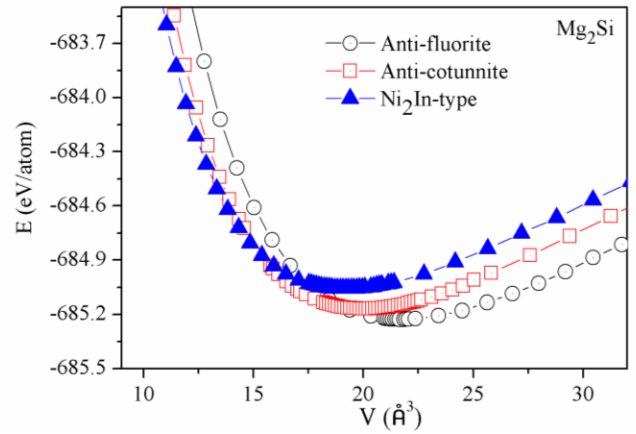


Fig. 1. The total energy of anti-fluorite, anti-cotunnite and Ni₂In-type structures Mg₂Si as a function of the volume

Table 1. Theoretical and experimental equilibrium parameters of anti-fluorite, anti-cotunnite and Ni₂In-type structures for Mg₂Si in zero pressure. a, b, c are lattice constant, v is volume

| Structures | | a (Å) | b (Å) | c (Å) | v (Å) ³ |
|-------------------------|----------|-------|-------|-------|--------------------|
| anti-fluorite | Present | 6.41 | 6.41 | 6.41 | 65.53 |
| | Exp [11] | 6.350 | 6.350 | 6.350 | 64.01 |
| | Cal [22] | 6.295 | 6.295 | 6.295 | 62.36 |
| anti-cotunnite | Present | 7.064 | 4.23 | 8.079 | 60.35 |
| | Exp [13] | 6.305 | 4.591 | 6.784 | 51.75 |
| | Cal [15] | 7.007 | 4.201 | 7.962 | 58.90 |
| Ni ₂ In-type | Present | 4.630 | 4.630 | 6.204 | 57.590 |
| | Exp [13] | 4.166 | 4.166 | 5.287 | 47.38 |
| | Cal [15] | 4.537 | 4.537 | 6.276 | 56.97 |

For a given pressure, the stable structure is the one whose Gibbs free energy has the lowest value. To determine the most stable structure at finite pressure and temperature, the Gibbs free energy given by $G = E + PV - TS$ should be used [23]. Since the calculations are

done at 0 K, the Gibb's free energy will become equal to the enthalpy $H = E + pV$. The enthalpy for the three different structures as a function of pressure is presented in Fig. 2. For a given pressure, the crystallographic phase with the lowest enthalpy is the most stable, and a crossing of two

curves indicates a phase transition induced by pressure. In Fig. 2, it is found that Mg_2Si transforms from the anti-fluorite structure to the anti-cotunnite structure at about 5.9 GPa, and when the pressure increases up to about 21.8 GPa, it transforms from the anti-cotunnite structure to the Ni_2In -type structure. The transformation pressures obtained are given in Table 2 along with previous experimental and other theoretical data [13, 15, 24]. Our result is agreement with experimental value, which indicates that the present method is quite successful.

Table 2. The transition pressures of anti-fluorite \rightarrow anti-cotunnite, anti-cotunnite $\rightarrow Ni_2In$ -type, compared with some compilation of experimental results and others' theoretical work

| | anti-fluorite to anti-cotunnite | anti-cotunnite to Ni_2In -type |
|--------------|---------------------------------|----------------------------------|
| Present | 5.9 GPa | 21.8 GPa |
| Exp [13, 24] | 7.5 GPa | 21.3 GPa |
| Cal [15] | 12.8 GPa | 19.6 GPa |

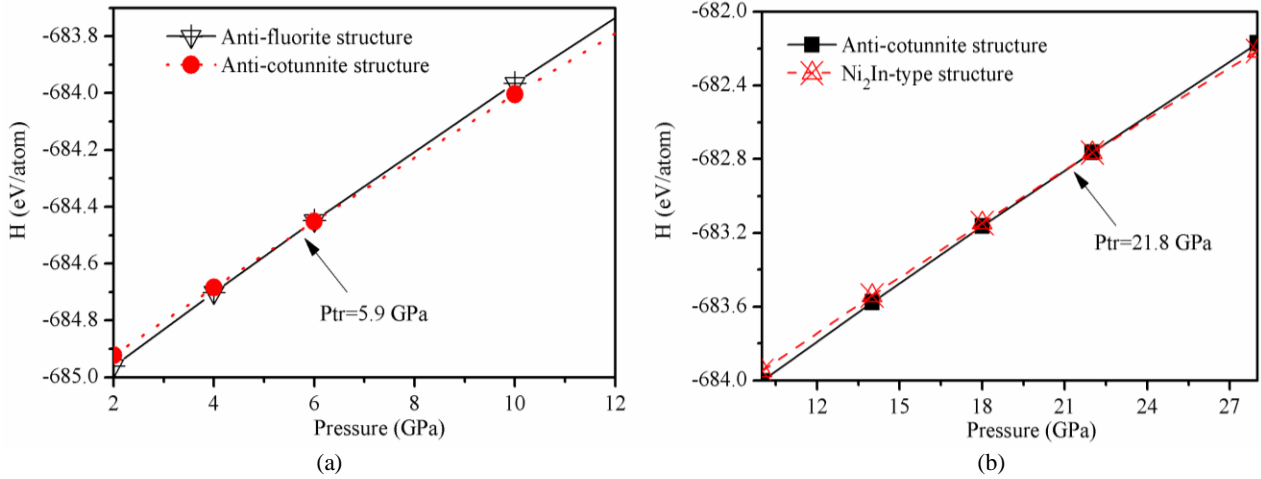


Fig. 2. (a) Enthalpy of anti-fluorite and anti-cotunnite structures Mg_2Si as a function of pressure, (b) Enthalpy of anti-cotunnite and Ni_2In -type structures Mg_2Si as a function of pressure

3.2. Elastic properties

The elastic stiffness determines the response of the crystal to an externally applied strain (or stress) and provides information about the bonding characteristics, mechanical and structural stability. The elastic behavior of a completely asymmetric material is specified by 21 independent elastic constants, while for an isotropic material, the number is 2. In between these limits the necessary number is determined by the symmetry of the material.

For cubic crystals, there are three independent elastic

constants, namely, C_{11} , C_{12} , and C_{44} . For orthorhombic crystals, there are nine independent elastic constants, namely, C_{11} , C_{22} , C_{33} , C_{44} , C_{55} , C_{66} , C_{12} , C_{13} , and C_{23} . Hexagonal crystals have five independent elastic constants C_{11} , C_{12} , C_{13} , C_{33} , and C_{44} . The elastic constants of three structures of Mg_2Si are listed in Table 3, 4, 5, respectively. We found that for three structures elastic constants increase with the increasing pressure. For anti-fluorite structure (see Table 3), our results are consistent with the experimental and other theoretical data [22, 25, 26]. There is no available experimental data and other theoretical results for the other two structures.

Table 3. The dependence of the elastic constants c_{ij} (given in GPa), elastic moduli B_H , G_H , E_H (GPa), the Poisson's ratio B_H/G_H and A on pressure for the anti-fluorite structure with some compilation of experimental results and others' theoretical work. (B_H/G_H as an indication of ductile vs brittle characters; A represents the degree of the anisotropy between the $\langle 100 \rangle$ and $\langle 110 \rangle$ directions)

| P (GPa) | | C_{11} (GPa) | C_{12} (GPa) | C_{44} (GPa) | B_H (GPa) | G_H (GPa) | E (GPa) | γ | G_H/B_H | A |
|---------|----------|----------------|----------------|----------------|-------------|-------------|-----------|----------|-----------|------|
| 0 | Present | 114.57 | 23.04 | 43.68 | 53.55 | 44.49 | 106.86 | 0.17 | 0.83 | 0.95 |
| | Cal.[25] | 113.5 | 22.8 | 43.2 | 53.1 | | | | | |
| | Exp.[26] | 126.0 | 26.0 | 48.5 | 59.0 | | | | | |
| 2 | Present | 124.36 | 29.42 | 50.36 | 61.06 | 49.19 | 113.08 | 0.19 | 0.80 | 1.06 |
| | Cal.[25] | 123.9 | 29.01 | 46.8 | 60.6 | | | | | |
| 4 | Present | 134.13 | 35.83 | 51.43 | 68.60 | 50.52 | 118.96 | 0.21 | 0.74 | 1.07 |
| | Cal.[25] | 133.7 | 35.2 | 49.7 | 68.0 | | | | | |
| 5.9 | Present | 143.34 | 42.18 | 54.64 | 75.91 | 52.92 | 124.14 | 0.23 | 0.69 | 1.08 |
| 8 | Present | 152.13 | 48.24 | 57.37 | 82.87 | 55.25 | 128.78 | 0.24 | 0.66 | 1.10 |

The calculated elastic constants allow us to obtain the macroscopic mechanical parameters of Mg₂Si compounds, namely their bulk (B) and shear (G) moduli. According to Hill [27], two main approximations, Voigt (V) [28] and Reuss (R) [29], are used. The bulk moduli (B_V , B_R) and the shear moduli (G_V , G_R) are obtained by calculated elastic constants and the literature gives detailed descriptions of the relationship [28-31].

Hill [27] has proven that the Voigt's and Reuss's equations represent upper and lower limits of realistic polycrystalline constants and has shown that the polycrystalline modulus is the arithmetic mean of Voigt's and Reuss's moduli, which is given by following equations:

$$G_H = \frac{1}{2}(G_V + G_R) \quad (1)$$

$$B_H = \frac{1}{2}(B_V + B_R) \quad (2)$$

Young's modulus E is defined as the ratio between stress and strain, and it can be used to provide a measure of the stiffness of the solid. The larger the value of E is, the stiffer the material is. The Poisson's ratio γ can quantify the stability of the crystal against shear, which usually ranges from -1 to 0.5. The larger the Poisson ratio is, the better the plasticity is [32].

To complete the physical elastic properties we have computed the polycrystalline Young's modulus (E) and the

Poisson's ratio γ from the Hill's values using the relationships [30].

$$E = \frac{9B_H G_H}{3B_H + G_H} \quad (3)$$

$$\gamma = \frac{3B_H - 2G_H}{2(3B_H + G_H)} \quad (4)$$

The pressure dependencies of the Young's modulus E, the Poisson's ratio (γ) of the anti-fluorite structure Mg₂Si are listed in Table 3, respectively, together with other theoretical results [25] and the experimental data [26]. From Table 3, one can find the calculated elastic modulus (B, G, E) and the Poisson's ratio (γ) agree well other theoretical results [25]. It is found that the calculated elastic modulus (B, G, E), and the Poisson's ratio (γ) increase gradually with increasing pressure, which indicates that pressure has an important effect on stress-strain properties of materials.

The calculated elastic constants and elastic modulus of anti-cotunnite and Ni₂In-type structures Mg₂Si are shown in Table 4 and 5, respectively. For anti-cotunnite and Ni₂In-type structures Mg₂Si, we also found that elastic modulus increase with applied pressures but no theoretical and experimental data are available.

Table 4. The dependence of the elastic constants c_{ij} (given in GPa), elastic moduli B_H , G_H , E_H (GPa), the Poisson's ratio γ , B_H/G_H and A on pressure for the anti-cotunnite structure. (B_H/G_H as an indication of ductile vs brittle characters; A1, A2, A3 represents the degree of the {100} ({010}, {001}) shear planes between the <011> and <010> (<101>, <001>, and <110>, <010>) directory, respectively)

| | 5.9 (GPa) | 8(GPa) | 12(GPa) | 16(GPa) | 20(GPa) | 21.8(GPa) |
|----------|-----------|--------|---------|---------|---------|-----------|
| C11(GPa) | 122.65 | 127.01 | 142.39 | 142.47 | 156.86 | 152.43 |
| C12(GPa) | 40.84 | 48.40 | 61.08 | 74.55 | 88.41 | 100.07 |
| C13 GPa) | 47.68 | 53.16 | 61.49 | 68.45 | 82.97 | 95.46 |
| C22 GPa) | 152.19 | 162.84 | 186.69 | 211.65 | 230.11 | 238.82 |
| C23 GPa) | 45.10 | 51.05 | 63.57 | 77.95 | 87.65 | 91.64 |
| C33 GPa) | 160.71 | 171.34 | 192.81 | 210.84 | 233.68 | 242.69 |
| C44(GPa) | 22.86 | 23.66 | 31.08 | 29.23 | 33.75 | 33.05 |
| C55 GPa) | 39.27 | 40.48 | 41.48 | 40.26 | 38.50 | 27.83 |
| C66 GPa) | 29.70 | 32.76 | 39.09 | 46.10 | 52.72 | 55.71 |
| BH (GPa) | 76.95 | 83.69 | 97.47 | 107.47 | 121.98 | 128.15 |
| GH (GPa) | 36.64 | 38.13 | 43.43 | 44.31 | 47.29 | 43.52 |
| E (GPa) | 94.86 | 99.31 | 113.44 | 116.87 | 125.63 | 117.28 |
| G/B | 0.48 | 0.46 | 0.45 | 0.41 | 0.39 | 0.34 |
| γ | 0.275 | 0.283 | 0.287 | 0.300 | 0.310 | 0.330 |
| A1 | 0.486 | 0.493 | 0.584 | 0.540 | 0.601 | 0.647 |
| A2 | 0.705 | 0.698 | 0.657 | 0.604 | 0.534 | 0.373 |
| A3 | 0.615 | 0.679 | 0.755 | 0.899 | 1.003 | 1.166 |

The shear modulus represents the resistance to plastic deformation while the bulk modulus represents resistance to fracture. Pugh [33] introduced the ratio of shear modulus to bulk modulus (G/B) of polycrystalline phases to predict the brittle and ductile behavior of materials. The critical value, which separates ductility from brittleness, is about 0.57. When G/B is smaller than 0.57, the materials are ductile; when G/B is larger than 0.57, the materials are brittle. The values obtained here B/G ratio are all greater than 0.57, which suggests that the anti-fluorite structure Mg_2Si is less ductile and much more brittle, and that the ductility strengthens with increasing pressure as a result of the augment of the B/G ratio with pressures. From Table 4 and 5, we can found that anti-cotunnite and Ni_2In -type structures Mg_2Si exhibit good ductility due to $G/B < 0.57$. Our results show that the anti-fluorite structures Mg_2Si is a semiconductor, while anti-cotunnite and Ni_2In -type structures Mg_2Si are metal (See Part 3.3). Because each ion in the metal is surrounded by the electron fluid in all directions, the bonding has no directional properties. This accounts for the high malleability and ductility of metals.

It is well known that microcracks are easily induced in the materials due to the elastic anisotropy. The shear anisotropic factors provide a measure of the degree of anisotropy in the bonding between atoms in different planes [34]. Hence, it is important to calculate elastic anisotropy in crystal structure in order to understand these properties and hopefully find mechanisms which will improve their durability. To quantify the anisotropy of elastic properties in Mg_2Si , the shear anisotropy ratios of the cubic anti-fluorite structure are calculated by [35]

$$A = \frac{2C_{44}}{C_{11} - C_{12}} \quad (5)$$

A represents the degree of the anisotropy between the $\langle 100 \rangle$ and $\langle 110 \rangle$ directions. In the case of isotropic crystals, A is equal to 1, while any value smaller or larger than 1 indicates anisotropy.

We present A with the change of the pressures in Table 3. It is found that the deviation from 1 increases with the increase of pressure. The results indicate that the cubic anti-fluorite structure Mg_2Si exhibits low elastic anisotropy at zero pressure and the degree of the anisotropy increases with increasing pressure.

For orthorhombic anti-cotunnite structure [30], the shear anisotropic factor for the $\{100\}$ between the $\langle 011 \rangle$ and $\langle 010 \rangle$ directory is

$$A1 = \frac{4C_{44}}{C_{11} + C_{33} - 2C_{13}} \quad (6)$$

For the $\{010\}$ planes between the $\langle 101 \rangle$ and $\langle 001 \rangle$ directory is

$$A2 = \frac{4C_{55}}{C_{22} + C_{33} - 2C_{23}} \quad (7)$$

For the $\{001\}$ planes between the $\langle 110 \rangle$ and $\langle 010 \rangle$ directory is

$$A3 = \frac{4C_{66}}{C_{11} + C_{22} - 2C_{12}} \quad (8)$$

The shear anisotropic factors are summarized in Table 4. In the case of isotropic crystals, the factors $A1$, $A2$, and $A3$ are equal to 1, while any value smaller or greater than one is a measure of the degree of elastic anisotropy possessed by the crystal. It is found that the value of $A1$ increases from 0.49 to 0.65 and $A3$ increases from 0.8 to 1.16 as the pressure is increased from 5.9 to 21.8 GPa. The results showed that, with increasing pressure, the anisotropy of anti-cotunnite structure Mg_2Si for $\{100\}$ planes between the the $\langle 011 \rangle$ and $\langle 010 \rangle$ directory increases, while the anisotropy of the structure for $\{001\}$ planes between the $\langle 110 \rangle$ and $\langle 010 \rangle$ directory decreases to a minimum and then increases. We found that $A2$ decreases with increasing pressure, which indicates that the anisotropy of anti-cotunnite structure Mg_2Si for $\{010\}$ planes between the $\langle 101 \rangle$ and $\langle 001 \rangle$ directory increases with increasing pressure.

For hexagonal Ni_2In -type structure, we have calculated the shear anisotropic factor (A) for the $\{10-10\}$ shear planes between $\langle 01-11 \rangle$ and $\langle 01-10 \rangle$ directions, which is identical to the shear anisotropy factor for the $\{10-10\}$ shear planes between $\langle 10-11 \rangle$ and $\langle 0001 \rangle$ directions [36]:

$$A = \frac{4C_{44}}{C_{11} + C_{33} - 2C_{13}} \quad (9)$$

The calculated shear anisotropic factors of Ni_2In -type structures Mg_2Si are given in Table 5. The value of A calculated is 0.58, indicating that Ni_2In -type structure Mg_2Si is characterized by anisotropy for the shear planes described above.

Table 5. The dependence of the elastic constants c_{ij} (given in GPa), elastic moduli B_H , G_H , E_H (GPa), the Poisson's ratio B_H/G_H and A on pressure for the Ni_2In -type structure Mg_2Si (B_H/G_H as an indication of ductile vs brittle characters; the A represents the degree of the anisotropy for the shear planes $\{10-10\}$ between $\langle 01-11 \rangle$ and $\langle 01-10 \rangle$ directions)

| | 21.8 (GPa) | 30 (GPa) |
|-----------|------------|----------|
| C11 (GPa) | 206.21 | 290.73 |
| C12 (GPa) | 117.06 | 146.87 |
| C13 (GPa) | 86.27 | 115.26 |
| C33 (GPa) | 207.38 | 294.03 |
| C44 (GPa) | 34.77 | 44.51 |
| C66 (GPa) | 43.71 | 70.54 |
| BH (GPa) | 132.43 | 180.59 |
| GH (GPa) | 43.14 | 62.43 |
| E | 116.74 | 167.93 |
| G/B | 0.32 | 0.34 |
| γ | 0.35 | 0.34 |
| A | 0.57 | 0.50 |

Once the elastic constants of the compound are known, one can calculate the Debye temperature at the low-temperature. The Debye temperature is a fundamental parameter of a material which is linked to many physical properties such as specific heat, elastic constants, and melting point [34]. It can be used to distinguish between high and low-temperature regions for a solid. For $T > \theta_D$ all modes have energy of $k_B T$ and for $T < \theta_D$ one expects high-frequency modes to be frozen [37]. The Debye temperature can be estimated from the average sound velocity v_m , by the following equation [38]

$$\Theta_D = \frac{h}{k} \left[\frac{3n}{4\pi} \left(\frac{N_A \rho}{M} \right) \right]^{1/3} v_m \quad (10)$$

where h is Planck's constants, k is Boltzmann's constant, N_A is Avogadro's number, n is the number of atoms in the molecule, M is the molecular weight, and ρ is the density. The average wave velocity v_m is approximately calculated from

$$v_m = \left[\frac{1}{3} \left(\frac{2}{v_s^3} + \frac{1}{v_p^3} \right) \right]^{-1/3} \quad (11)$$

where v_p and v_s are the compressional and shear wave velocities, respectively, which can be obtained from equation [35]

$$v_p = \sqrt{\left(B + \frac{4}{3} G \right) \frac{1}{\rho}} \quad (12)$$

$$v_s = \sqrt{\frac{G}{\rho}} \quad (13)$$

The obtained compressional, shear, average wave velocities and Debye temperatures are shown in the Table 6, 7, and 8, respectively. At zero pressure and zero temperature, the obtained compression and shear wave velocities of the cubic anti-fluorite structure Mg₂Si agree with the other calculated result [32]. We obtain $\theta_D = 562.66$ K, which agrees well with experimental values ($\theta_D = 528.45$ K) [39]. From the Table 6, it is shown that the v_p , v_s , v_m and Debye temperatures θ_D of the cubic anti-fluorite structure Mg₂Si increase with increasing pressure. We also found that the Debye temperatures θ_D for anti-cotunnite structure Mg₂Si is larger than that of Ni₂In-type structure Mg₂Si. From Table 7, it was found that the Debye temperature Fig. 1. The total energy of anti-fluorite, anti-cotunnite and Ni₂In-type structures Mg₂Si as a function of the volume for anti-cotunnite structure Mg₂Si increases with increasing pressure, reach their maximum value at about 20GPa, and then decrease with pressure increased further. The results indicated that the Debye temperature θ_D of Ni₂In-type structures Mg₂Si also increases with increasing pressure (see Table 8). There are no available theoretical and experimental results

for anti-cotunnite and Ni₂In-type structures Mg₂Si.

Table 6. The pressure-dependence of longitudinal, transverse, average sound velocities (v_p , v_s and v_m in m/s), and Debye temperature (θ_D in Kelvin) for the anti-fluorite structure Mg₂Si, with some experimental results and others' theoretical work

| P (GPa) | | v_t | v_l | v_m | θ_D |
|---------|----------|---------|--------|--------|------------|
| 0 | Present | 4.7832 | 7.6187 | 5.2666 | 562.66 |
| | Cal [32] | 4.8657 | 7.7225 | 5.8167 | |
| | Exp [40] | | | | 528.45 |
| 2 | | 4.95404 | 7.9491 | 5.4591 | 589.13 |
| 4 | | 4.95038 | 8.1210 | 5.4677 | 595.63 |
| 5.9 | | 4.99005 | 8.3018 | 5.5192 | 607.38 |
| 8 | | 5.03497 | 8.4749 | 5.5752 | 618.71 |

Table 7. The pressure-dependence of longitudinal, transverse, average sound velocities (v_p , v_s and v_m in m/s), and Debye temperature (θ_D in Kelvin) for the anti-cotunnite structure Mg₂Si

| P (GPa) | v_t | v_l | v_m | θ_D |
|---------|--------|--------|---------|------------|
| 5.9 | 3.9925 | 7.3979 | 4.4564 | 503.41 |
| 8 | 4.0229 | 7.5564 | 4.4947 | 511.93 |
| 12 | 4.1993 | 7.9428 | 4.6941 | 542.60 |
| 16 | 4.1614 | 8.0679 | 4.6594 | 545.48 |
| 20 | 4.2269 | 8.3611 | 4.73867 | 561.06 |
| 21.8 | 4.0176 | 8.3097 | 4.5155 | 537.94 |

Table 8. The pressure-dependence of longitudinal, transverse, average sound velocities (v_p , v_s and v_m in m/s), and Debye temperature (θ_D in Kelvin) for the Ni₂In-type structure Mg₂Si

| P(GPa) | v_t | v_l | v_m | θ_D |
|--------|--------|--------|--------|------------|
| 21.8 | 3.9187 | 8.2229 | 4.4077 | 532.34 |
| 30 | 4.4983 | 9.2472 | 5.0540 | 629.77 |

3.3. Electronic properties

The band structures of the anti-fluorite structure of Mg₂Si along high symmetry directions are presented in Fig. 3. It indicates that the anti-fluorite structure of Mg₂Si is indirect gap semiconductor. The valence band maximum is located at the Γ point, whereas the conduction band minimum is located at the X point. The valence-band maximum is made up by a twofold degenerate band at the Γ point. Away from Γ these split into a light band and a heavier bands, which are approximately parabolic near G

but become more weakly dispersive as one moves away from the zone center. Thus the valence bands for p-type doping show a combination of heavy and light bands, which has been previously discussed as favorable for thermoelectric performance [40, 41].

The fundamental GGA band gap of the anti-fluorite structure of Mg_2Si is about 0.22 eV, which is smaller than the values of the experiment (0.69 eV) [42] and is agreement with the previous other DFT calculations (0.21 eV) [43]. The underestimation of the band gap is a known deficiency of the DFT calculation. The problem can be alleviated by using more elaborate but time consuming methods. It has been shown that a quasiparticle calculation within the GW approximation works well in predicting the band gap values [44]. Arnaud and Alouani [45] obtained the band gap of 0.65 eV for Mg_2Si that agreed fairly well with experiments.

Fig 4 (a) displays the total density of states (DOS) of Mg_2Si , where the dotted line is the Fermi level (E_F). From Fig. 4 (a), we found that the DOS increases rapidly away from the band edge for both the valence and conduction bands, meaning that as far as the increase of the DOS away from the band edge, both the conduction and valence bands show heavy features that all things being equal

would be similarly favorable for thermoelectric performance [46].

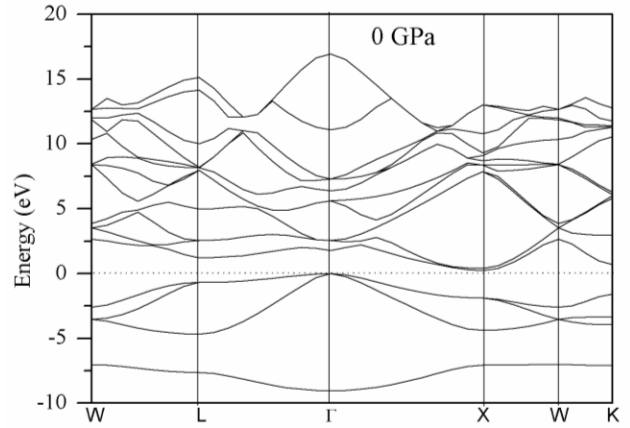


Fig. 3. The band structure for anti-fluorite structure Mg_2Si . The Fermi level is set to 0 eV, which is the top of the valence band

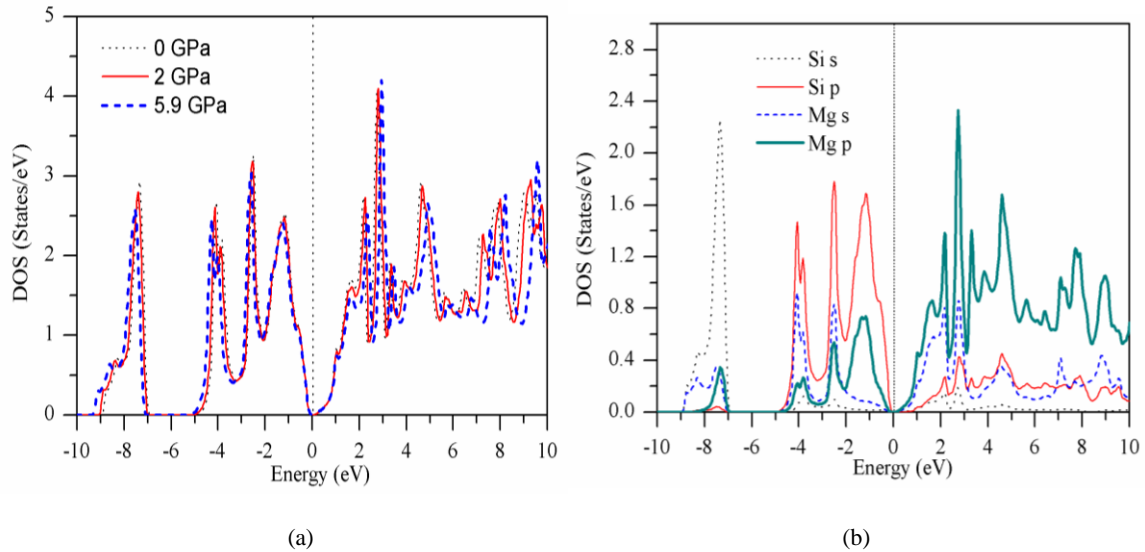


Fig. 4. (a) The total density of states at different pressures. (b) Partial densities of states of Mg_2Si projected onto the s and p orbitals of Mg and Si for the anti-fluorite structure at zero pressure, where the dotted line is the Fermi level (E_F)

In general, s and p orbitals are rather extended and overlap between sites. This can make the assignment of orbital character to band states ambiguous. However, this can be addressed in part by projecting onto small spheres, as was discussed in the context of hydrides [47].

Partial densities of states of Mg_2Si projected onto the s and p orbitals of Mg and Si for the anti-fluorite structure at zero pressure (see Fig. 4(b)). It is found that Si 3s orbitals are at high binding energy, forming a narrow band ~ 8 eV below the valence-band maximum. The valence band is mainly due to the hybridization between Mg 2p and Si 3p states and is rather narrow, with a total width of slightly more than 4 eV. The lowest conduction band of

Mg_2Si is mainly dominated by 2p and 3s states of Mg atoms. The results indicated that the valence bands have stronger Si 3p character, while the conduction bands have stronger Mg character, indicating charge transfer from Mg to Si, consistent with the fact that Si is substantially more electronegative than Mg [46]. Since the transport properties are mainly dictated by the DOS around the Fermi level, the valence p states of the Si and the conduction p states of Mg are predominantly responsible for the transport properties of Mg_2Si .

Study indicated that pressure tuning plays an important role in the magnitude of the thermoelectric power and band structure calculations can be a good tool

to increase the rate of discovery of improved thermoelectric materials [48].

From Fig. 5 we found that with the increase of pressure the band gap gradually decreases from 0.22 to 0.11 eV. Although the DFT-GGA calculations underestimate the energy bandgaps, they generally predict the correct qualitative behavior. It is revealed (see Fig. 5) that the conduction band minimum (CBM) shifts forward to lower energy with the increase of pressure, which results in the decrease of the band gap. According to our calculations, the lowest conduction bands are mainly occupied by the 2p orbitals of Mg, and to a much smaller

extent by the 3p orbitals of Si. It is found that from Fig. 6 the contribution to lowest conduction bands from Si 3p orbitals states increases with the increase of pressure, which results in the increase of coupling between the orbitals of Si and the orbitals of Mg. So the conduction widths increase with increasing pressure, which results in the decrease of the band gap. This is consistent with the results given by Kalarese and Bennecer [49]. Their calculation results show that the anti-fluorite Mg_2Si has become metallic under pressure due to the presence of Mg-Si bonds.

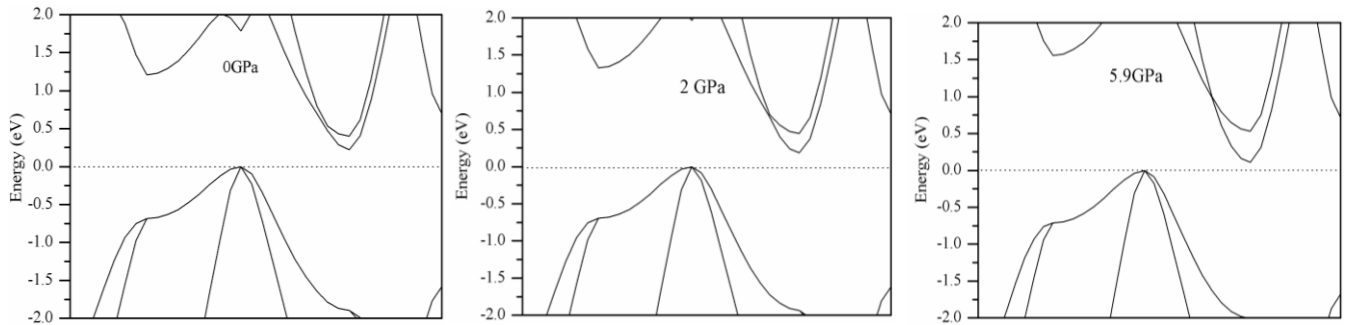


Fig. 5. The band-edge structure of the anti-fluorite structure Mg_2Si under different pressures

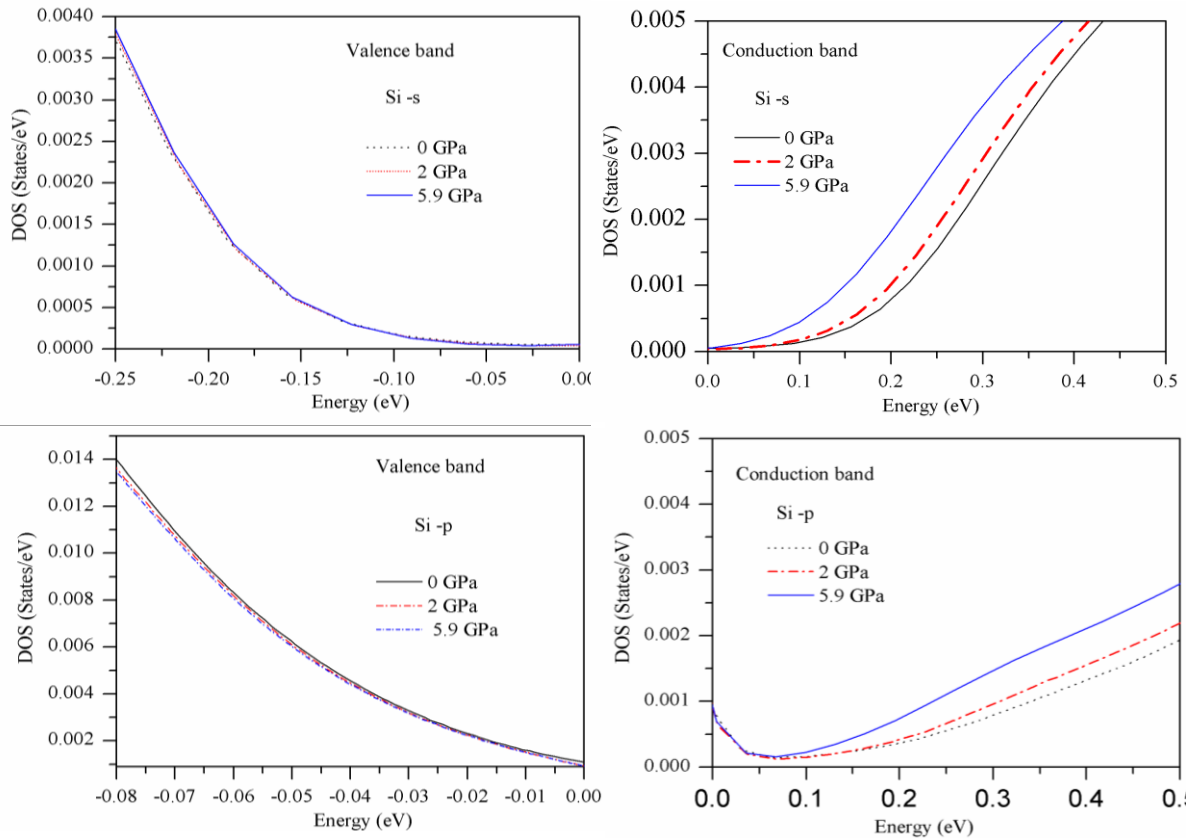


Fig. 6. Partial densities of states of Mg_2Si projected onto the s and p orbitals of Si for the anti-fluorite structure under different pressure

If we focus on the band edge (see Fig. 5), we see that the valence bands are similar but different in the lowest conduction bands under different pressure. It is found for anti-fluorite structure that the pressure leads to the change in the energy dispersion of lowest conduction band but the energy dispersion relations of top of the valence band hardly be affected.

Changes in the band structures can be easily explained from the analysis of the density of partial states. Fig. 6 shows that the contribution to valence band near the Fermi level from s states and p states of Si has hardly changed, but the contribution to lowest conduction bands from Si 3p orbitals states increases with pressure. This indicates that the conduction bands of the anti-fluorite structure are influenced by the pressure whereas the valence bands are not much affected.

The change in thermoelectric power must be related to the details of the change in the electronic structure near the Fermi energy [50]. Chasmar *et al.* [51] have investigated

the optimum gap of a thermoelectric semiconductor by calculations and found that the band gap can influence the thermoelectric properties significantly. These results indicate that it is possible to improve thermoelectric properties by means of pressure tuning. Martin *et al.* [18] also suggest that once improved TE behavior is found by means of pressure tuning, attempts can be made to reproduce this behavior by means of chemical tuning, or by other means.

The electronic band structure of the anti-cotunnite and Ni_2In -type structures are shown in Fig. 7. It indicates that the two materials exhibit metallic behavior with several overlaps between the conduction bands and the valence bands. As pressure increases, the overlap becomes stronger (we did not present figure). The studies indicated that two different factors determine the response of materials to pressure: (a) changes in nearest-neighbor distance and (b) changes in symmetry [52].

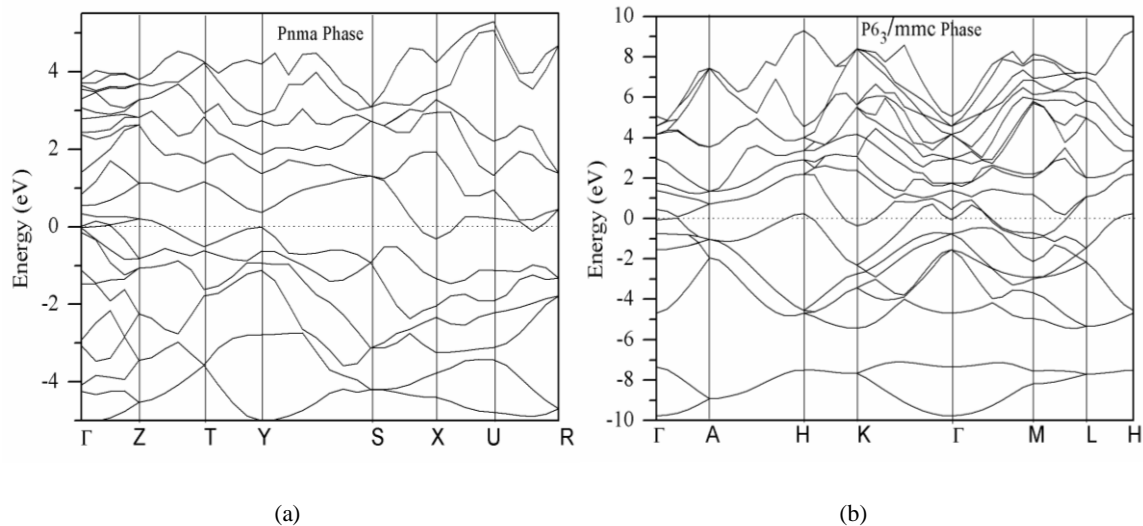


Fig. 7. The band structure, (a) for the anti-cotunnite structures Mg_2Si , (b) Ni_2In -type structures Mg_2Si

4. Conclusions

In the present study, the lattice parameters, phase transition, the elastic properties, the electronic properties of Mg_2Si under high pressures are investigated by first-principles calculations. The results indicate that Mg_2Si undergoes two phase transitions from anti-fluorite to anti-cotunnite at 5.9 GPa, and from anti-cotunnite to the Ni_2In -type structure at 21.8 GPa. It is found that the anti-fluorite structures Mg_2Si are brittle but the anti-cotunnite and Ni_2In -type structures Mg_2Si exhibits good ductility. We found that pressure has an important effect on stress-strain properties and Debye temperatures in three structures Mg_2Si . Calculations indicate that the band gap of anti-fluorite structure gradually decreases from 0.22 to 0.11 eV with the increase of pressure. Moreover, for anti-fluorite structure Mg_2Si , it is found that the pressure leads to the change in the energy dispersion of

lowest conduction band but the energy dispersion relations of the valence band top hardly be changed.

Acknowledgments

This work was supported by Yunnan province department of education fund (No. 2014Z143).

References

- [1] G. H. Li, H. S. Gill, R. A. Varin, *Metall. Trans. A* **24**, 2383 (1993).
- [2] V. K. Zaitsev, M. I. Fedorov, E. A. Gurieva, I. S. Eremin, P. P. Konstantinov, A. Y. Samunin, M. V. Vedernikov, *Phys. Rev. B* **74**, 045207 (2006).
- [3] Q. Zhang, J. He, J. Zhu, S. N. Zhang, X. B. Zhao, T.

- M. Tritt, *Appl. Phys. Lett.* **93**, 102109 (2008).
- [4] G. S. Nolas, D. Wang, M. Beekman, *Phys. Rev. B* **76**, 235204 (2007).
- [5] T. Dasgupta, C. Stiewe, R. Hassdorf, A. J. Zhou, L. Boettcher, E. Mueller, *Phys. Rev. B* **83**, 235207 (2011).
- [6] W. Liu, X. J. Tan, K. Yin, H. J. Liu, X. F. Tang, J. Shi, Q. J. Zhang, C. Uher, *Phys. Rev. Lett.* **108**, 166601 (2012).
- [7] R. Saravanan, M. C. Robert, *J. Alloys Compd.* **479**, 26 (2009).
- [8] J. I. Tani, H. Kido, *Intermetallics* **15**, 1202 (2007).
- [9] R. Song, L. Yazheng, A. Tatsuhiko, *J. Mater. Sci. Technol.* **21**, 618 (2005).
- [10] E. J. Guo, B. X. Ma, L. P. Wang, *J. Mater. Process. Technol.* **206**, 161 (2008).
- [11] J. Zhang, Z. Fan, Y. Q. Wang, B. L. Zhou, *Mater. Sci. Eng. A* **281**, 104 (2000).
- [12] P. Cannon, E. T. Conlin, *Science* **145**, 487 (1964).
- [13] J. Hao, B. Zou, P. W. Zhu, C. X. Gao, Y. W. Li, D. Liu, K. Wang, W. W. Lei, Q. L. Cui, G. T. Zou, *Solid State Commun.* **149**, 689 (2009).
- [14] F. Yua, J. X. Sun, W. Yang, R. G. Tian, G. F. Ji, *Solid State Commun.* **150**, 620 (2010).
- [15] H. H. Jun, G. G. Zhi, H. J. Qing, *Solid State Commun.* **150**, 2299 (2010).
- [16] J. F. Meng, N. C. Shekar, D. Y. Chung, M. Kanatzidis, J. Badding, *J. Appl. Phys.* **94**, 4485 (2003).
- [17] J. F. Meng, N. C. Shekar, J. V. Badding, D. Y. Chung, M. Kanatzidis, *J. Appl. Phys.* **90**, 2836 (2001).
- [18] J. Martin, G. S. Nolas, H. Wang, J. Yang, *J. Appl. Phys.* **102**, 103719 (2007).
- [19] M. C. Payne, M. P. Teter, D. C. Allan, T. A. Arias, J. D. Joannopou, *Rev. Modern Phys.* **64**, 1045 (1992).
- [20] J. P. Perdew, K. Burke, M. Ernzerhof, *Phys. Rev. Lett.* **77**, 3865 (1996).
- [21] H. J. Monkhorst, J. D. Pack, *Phys. Rev. B* **13**, 5188 (1976).
- [22] J. I. Tani, H. Kido, *Comput. Mater. Sci.* **42**, 531 (2008).
- [23] O. K. Andersen, O. Jepsen, *Phys. Rev. Lett.* **53**, 2571 (1984).
- [24] J. Hao, *Studies on the characteristics and structure transformation of magnesium silicide under high pressure*, Jilin University, 2008.
- [25] B. H. Yu, D. Chen, Q. B. Tang, C. L. Wang, D. H. Shi, *J. Phys. Chem. Solids* **71**, 758 (2010).
- [26] O. Madelung, L. Bornstein, *Numerical Data and Functional Relationships in Science and Technology, New Series, Group III*, **17e**, Springer-Verlag, Berlin 163, 432 (1983).
- [27] R. Hill, *Proc. Phys. Soc. Lond. A* **65**, 349 (1952).
- [28] W. Voigt, *Lehrbuch der Kristallphysik*. Teubner, Leipzig, 1928.
- [29] A. Reuss, *Z. Angew. Math. Mech.* **9**, 49 (1929).
- [30] D. Connétable, O. Thomas, *Phys. Rev. B* **79**, 094101 (2009).
- [31] M. B. Kanoun, S. G. Said, A. H. Reshak, A. E. Merad, *Solid State Sci.* **12**, 887 (2010).
- [32] Z. W. Huang, Y. H. Zhao, H. Hou, P. D. Han, *Physica B* **407**, 1075 (2012).
- [33] S. F. Pugh, *Philos. Mag.* **45**, 823 (1954).
- [34] P. Ravindran, L. Fast, P. A. Korzhavyi, B. Johansson, J. Wills, O. Eriksson, *J. Appl. Phys.* **84**, 4891 (1998).
- [35] K. B. Panda, K. S. Chandran, *Comput. Mater. Sci.* **35**, 134 (2006).
- [36] Z. Sun, S. Li, R. Ahuja, J. M. Schneider, *Solid State Commun.* **129**, 589 (2004).
- [37] B. Mayer, H. Anton, E. Bolt, *Intermetallics* **11**, 23 (2003).
- [38] O. L. Anderson, *J. Phys. Chem. Solids* **24**, 909 (1963).
- [39] D. W. Zhou, J. S. Liu, S. H. Xu, *Comput. Mater. Sci.* **51**, 409 (2012).
- [40] D. Parker, D. J. Singh, *Phys. Rev. B* **82**, 035204 (2010).
- [41] D. J. Singh, I. I. Mazin, *Phys. Rev. B* **56**, R1650 (1997).
- [42] A. Stella, D. W. Lynch, *J. Phys. Chem. Solids* **25**, 1253 (1964).
- [43] H. F. Wang, W. G. Chu, H. Jin, *Comput. Mater. Sci.* **60**, 224 (2012).
- [44] M. Hybertsen, S. G. Louie, *Phys. Rev. B* **34**, 5390 (1985).
- [45] B. Arnaud, M. Alouani, *Phys. Rev. B* **64**, 033202 (2001).
- [46] J. J. Pulikkotil, D. J. Singh, S. Auluck, M. Saravanan, D. K. Misra, A. Dhar, R. C. Budhani, *Phys. Rev. B* **86**, 155204 (2012).
- [47] H. Takenaka, D. J. Singh, *Phys. Rev. B* **75**, 241102 (2007).
- [48] J. F. Meng, N. V. Shekar, J. V. Badding, G. S. Nolas, *J. Appl. Phys.* **89**, 1730 (2001).
- [49] F. Kalarasse, B. Bennecer, *J. Phys. Chem. Solids* **69**, 1775 (2008).
- [50] N. P. Blake, S. Lattner, J. D. Bryan, G. D. Stucky, H. Metiu, *J. Chem. Phys.* **115**, 8060 (2001).
- [51] R. Chasmar, R. Stratton, *J. Electron. Control* **7**, 52 (1959).
- [52] L. Mancera, J. Rodríguez, N. Takeuchi, *J. Phys.: Condens. Matter.* **15**, 2625 (2003).

^{*}Corresponding author: SKdeng@126.com